The complex interplay between adsorption and photoactivity in hybrids rGO/TiO2

The complex interplay between adsorption and photoactivity in hybrids rGO/TiO_2

M. Minella, F. Bertaina, C. Minero*

Department of Chemistry and NIS Center of Excellence, University of Torino, Via P. Giuria 5, Torino 10125, Italy, http://www.environmentalchemistry.unito.it.

* Corresponding author. Fax +39-011-6705242; E-mail: claudio.minero@unito.it.

The kinetic of photocatalytic degradation of 2,4-DCP and 1-Naphthol on hybrids TiO_2/reduced-Graphene Oxide (TiO_2/rGO) obtained with two commercial TiO_2 specimens and different % rGO loadings was investigated under different irradiation conditions (UV only, UV + Vis and Vis only). 2,4-DCP adsorbs strongly on the rGO phase. With the increment of the rGO loading no increment on the overall reaction rate under UV and UV + Vis irradiation is observed, while a very low but not null photoactivity that increases with the increment of %rGO is observed under Vis only irradiation.

It is here proposed for the first time a quantitative kinetic model able to predict the photocatalytic rate of hybrid photocatalysts composed of two phases (whatever the nature of the phases is) with different light absorption and intrinsic reactivity, diverse ability to adsorb the substrate and to partition charge carriers depending on their band alignment. The model is able to decouple the adsorption effect from the kinetic ones.

From the analysis of the adsorption and kinetic data at different rGO loadings emerges that: 2,4-DCP partitions preferentially on the rGO phase; the operational photocatalytic mechanism is based on the band-to-band transition promoted by the UV absorption of the semiconductor; rGO shows a negligible but not null visible photoactivity toward 2,4-DCP; the photo-promoted TiO_2 conduction band electrons are not injected into rGO where 2,4-DCP is mainly adsorbed. In this light some hypothesis are proposed to justify the negative effect of rGO on the overall oxidative photoactivity.

Keywords

Photocatalysis, graphene oxide, titanium dioxide, adsorption, hybrid material, 2,4-dichlorophenol

1 Introduction

The investigation of the photocatalytic process under irradiated semiconductors has been mainly finalized to *i*) the discovery of new materials able to activate the photocatalytic process with high quantum yield and *ii*) the modification of the original materials with the aim to increase the utilization of light. Among the strategies directed to increase the overall photocatalytic performance, the synthesis of hybrid materials is one of the most explored fields, as recently highlighted.[1] A hybrid material is composed by two or more strongly interacting phases. Its features are not the sum of the properties of the single phases, but derive from their synergistic interaction and are strongly related to the properties of the interface between the materials. In this light not only the relative positioning of the electronic bands of materials, but also their structural matching (and the consequent presence of crystallographic defects) play a crucial role on the kinetic of separation of photogenerated charge carriers and on recombination phenomena. Therefore, also the spectroscopic features of a hybrid material are not generally the sum of the spectroscopic properties of the two materials although weighted for their relative amount in the hybrid, but derive from more complex interactions.

The increase of substrate adsorption can be an effective way to increase the performance when the photogenerated reactive charges (holes or electrons) are able to migrate and react on the adsorption phase.[2] The increment of the adsorption ability cannot be considered an *a priori* beneficial feature, because the partitioning of a substrate on a non-reactive phase can depress the efficiency of the process.

Among the different carbon based materials, TiO_2/graphene or TiO_2/graphene-like materials play a dominant role (to deepen the knowledge of this topic please refer to [3,4,5]). Recently, experiments with hybrids composed by functionalized graphene nanoparticles (GNPs) and TiO_2 exposing predominantly {101} facets showed that the proximity between the {101} facets and the carboxylated GNPs led to a more efficient injection of photoelectrons, decreased the kinetic of recombination, and improved the degradation of phenol.[6] Huang et al. compared photoluminescence (PL) of pristine TiO_2, mechanical mixture TiO_2/rGO and chemically bonded composite and reported that only in the presence of a chemical link between the organic and inorganic phases a significant decrement in the PL emission was observed. The decrement was correlated with a better charge carriers transfer and separation as a consequence of the electron transfer promoted by the presence of pure graphene.[7]

From the photocatalytic point of view, the role of rGO in TiO_2/rGO hybrids has not yet totally elucidated. The role of rGO as conductive “bridge” was proposed by Lang et al. [8] which concluded that in hybrid systems, in which Ag nanocubes and thin TiO_2 nanocrystals with preferentially exposed (001) facets were co-deposited on the surface of rGO nanosheets, rGO transports electrons from Ag to TiO_2. Recently, rGO nanosheets in MoS_X-rGO/TiO_2 have been proposed to transfer photogenerated electrons from the conduction band of TiO_2 to MoS_X where the reduction of H^+ to H_2 occurred.[9,10] Hamandi et al. reported that rGO can act as final electron acceptor in ternary hybrids composed by anatase, rutile and rGO.[11] Yang et al. reported that TiO_2/Ag_3PO_4/graphene composites showed not only the commonly reported visible activity toward the decomposition of organic dyes, but also a strong ability to inactivate bacteria.[12] The same increment in the photo-assisted decomposition of organic

dyes (e.g. Methyl Orange) has been recently reported on electrospun rGO/TiO_2 composite nanofibers.[13]

The role of electron acceptor for rGO in TiO_2-rGO composites has been correlated by Morawski et al. [14] to the presence of oxygen sites of rGO that are able to accept photoinduced electrons during the photocatalytic degradation of acetic acid under visible light. The stability of rGO alone [15] or coupled with TiO_2 [16] was also investigated, demonstrating the vulnerability of rGO (till its mineralization) in photocatalytic conditions. This raised concerns regarding its use in many applications where strong oxidants ($^{\bullet}OH$ and/or h^{+}_{vb}) are likely to be formed. Regarding the nature of the photo-formed oxidative species in TiO_2/rGO, a central role of the h^{+}_{vb} than $^{\bullet}OH$ radicals was proposed even for the oxidation of dyes,[17] in agreement with the general downsizing of the importance of free $^{\bullet}OH$ in solution even under pristine TiO_2.[18]

A critical review of the problems related to the interpretation of basic phenomena occurring in the hybrids TiO_2-rGO indicated several controversies on the sensitization by visible light and the role of graphene.[19] An in-depth study of the photocatalytic properties of TiO_2-rGO hybrids through a systematic investigation of the photocatalytic transformation of both phenol and methylene blue (MB) was carried out. The conclusions were that the former is mainly transformed via UV-based photocatalysis and that rGO decreases the phenol transformation rate because it depresses the amount of light reaching the semiconducting phase through the increase of the UV scattering ability. MB is transformed both via UV-based photocatalysis and in the case of visible irradiation via a dye-sensitized mechanism, while an effective Visible sensitization seems not to be the main mechanism. This study supported that electron transfer can occur from photoexcited states of rGO onto the TiO_2 and hole transfer from TiO_2 to rGO where adsorbed substrates can be oxidized only if thermodynamic requirements are satisfied (HOMO higher in energy than the empty states (h^{+}_{rGO}) of excited rGO).[19]

The aim of this work was the study of the photocatalytic properties of TiO_2/rGO hybrid materials synthetized with a reported hydrothermal treatment, through a detailed investigation of their photocatalytic activity toward 2,4-dichlorophenol, a substrate able to react not only through the oxidative pathway (promoted by photo-produced holes), but also through reductive pathway. To give insights into the mechanism and to investigate the role of the rGO phase, the degradation of 2,4-DCP was carried out on materials with different rGO loadings, at different substrate concentrations and under different irradiation sources. The role of the type of TiO_2 used was considered using hybrid materials synthesized with two different commercial TiO_2 powders. The TiO_2-rGO hybrids reactivity was also tested using 1-naphthol, which cannot be transformed through reductive pathways, and with hybrid materials synthesized through an alternative synthetic way (chemical reduction of GO).

2 Materials and Methods

2.1 Materials

All the compounds were used as received without any further purification step. The water solutions were prepared with water of MilliQ grade (TOC = 2 ppb, conductivity 18.2 MΩ cm).

Acetonitrile (gradient grade), H_3PO_4 (85%), HNO_3 (≥65%), H_2O_2 (35%), 2,4-dichlorophenol (2,4-DCP, 99%), 1-naphthol (99%) and hydrazine monohydrate (N_2H_4 64-65 %, reagent grade 98%) were purchased from Sigma-Aldrich; H_2SO_4 (96%), $KMnO_4$ (>99%) from Carlo Erba Reagenti (Italy); graphite natural powder (briquetting grade, ≈ 100 mesh, 99.9995%) from Alfa Aesar and zero-grade air for TOC analysis from Sapio (Turin, Italy). The commercial TiO_2 used for the synthesis of the hybrid TiO_2-rGO materials were *i*) TiO_2 Hombikat N100 (100% anatase, BET specific surface area 100 m^2 g^{-1}, average crystal size 20 nm) and *ii*) P25 (Evonik-Degussa, 70% anatase – 30% rutile, 50 m^2 g^{-1}, plate-like particles with mean size ca. 40 nm).

2.2 GO and TiO_2-rGO synthesis

The graphene oxide was produced through the modified Hummers and Staudemaier's method [20] proposed by Huang et al. [21] and described in detail elsewhere [22]. The absorption spectra of the GO suspension properly diluted (see Fig. 1A-SM of the Supplementary Material, here after SM) were recorded through a UV/Vis Varian Cary 100 spectrophotometer in the 200-800 nm range. The spectrum showed the classic absorption profile of GO [15,21,23] characterized by a peak at 230 nm ($\pi \rightarrow \pi^*$ transition of the C=C double bonds) with a shoulder at $\lambda \approx 300$ nm ($n \rightarrow \pi^*$ transition of carbonyl groups).[23,24] The concentration of the suspension in term of mass of carbon per mass of solution was evaluated measuring Total Organic Carbon (TOC) concentration of diluted solutions of the GO. The TOC analyzer adopted was a Shimadzu TOC-VCSH Total Organic Carbon Analyzer, equipped with an ASI-V autosampler and fed with zero-grade air.

The hybrids TiO_2-rGO were produced following literature procedures [25,26,27] through reduction of different amount of GO onto the TiO_2 nanoparticles. In the hydrothermal treatment the autogenous pressure inside a sealed autoclave induced an effective reduction of the oxidized moieties of GO to give rGO. We added drop by drop different volumes of the GO suspension to 4 g dm^{-3} suspensions of TiO_2 (N100 or P25) under constant and vigorous magnetic stirring. The addition of GO to the suspension destabilized the colloid as a consequence of the strong interaction between the organic and inorganic phase that promoted the coagulation of the particles. The as obtained suspension was transferred in a 1 dm^3 Teflon vessel and hydrothermally treated in a Berghof DAB 3 autoclave according to the temperature ramp profile reported in Fig. 2-SM. At the end of the hydrothermal treatment a grey to dark-grey suspension was obtained as a function of the rGO loading. The suspension was filtered on 0.45 μm hydrophilic filters (Whatman, NL 17 membrane filters, polyamide), washed with water and dried at 373 K in oven. Materials with %rGO loadings equal to 0.5, 1, 2, 4, 6, 10 and 20% were produced with N100, while hybrids with %rGO loading equal to 4, 6 and 10% with P25. The rGO loading was computed considering a complete conversion of all the carbon of the GO in rGO without any loss of carbon during the hydrothermal reduction.

The chemical reduction of GO to rGO was carried out using hydrazine according to the proposed method.[19] An in-depth characterization of the catalysts here investigated from a physico-chemical point of view has been previously reported.[19,22]

In this work *n*%rGO(*X*)-*Y* identifies univocally the catalysts, where *n* is the rGO loading in %, *X* is the type of process carried out to reduce the GO to rGO (*HTR* = HydroThermal Reduction, *CR* = Chemical Reduction) and *Y* is the type of titanium dioxide employed (*N100* = TiO_2 Hombikat N100, *P25* = TiO_2 Evonik P25).

2.3 Photocatalytic conditions and analytical determinations

The photocatalytic experiments were carried out in cylindrical Pyrex glass cells (dimensions: 4.0 cm diameter and 2.5 cm height; cut-off at 295 nm) on 5 cm^3 of suspension with the desired amount of the organic substrate to be degraded (e.g. 2,4-DCP), 0.5 g dm^{-3} catalyst suspension at pH 3 for HNO_3. The suspensions were prepared and left in dark for at least 2 hours, measuring the concentration in solution until the adsorption equilibrium was attained. During the irradiation the cells were magnetically stirred. The temperature of the cells was kept constant at 30±3 °C. At defined irradiation times the suspension was filtered on 0.45 μm cellulose acetate membrane filter (Millipore HA) and HPLC-UV analyzed.

The concentration of 2,4-DCP and 1-naphthol was measured through a YL HPLC system 9300 with a YL9330 Column Compartment and a YL9150 autosampler. The column was a RP C18 LiChroCART® - LiChrosphere® with 5 μm particles. The detection was carried out at 210 nm and 220 nm for 2,4-DCP and 1-naphthol, respectively. The elution was carried out in isocratic mode at 1 cm^3 min^{-1} with H_3PO_4 4.2 mM/acetonitrile 55:45 or 65:35 for 2,4-DCP and 1-naphthol, respectively. The retention time of 2,4-DCP under the adopted conditions was 5.5 minutes and for 1-napthol 8.9 min. The injection volume was 60 μL for both substrates. In all the photocatalytic degradation experiments an exponential decay of the concentration was observed. From the fitting the pseudo-first order kinetic constants (k_{obs}) for the photocatalytic process was obtained.

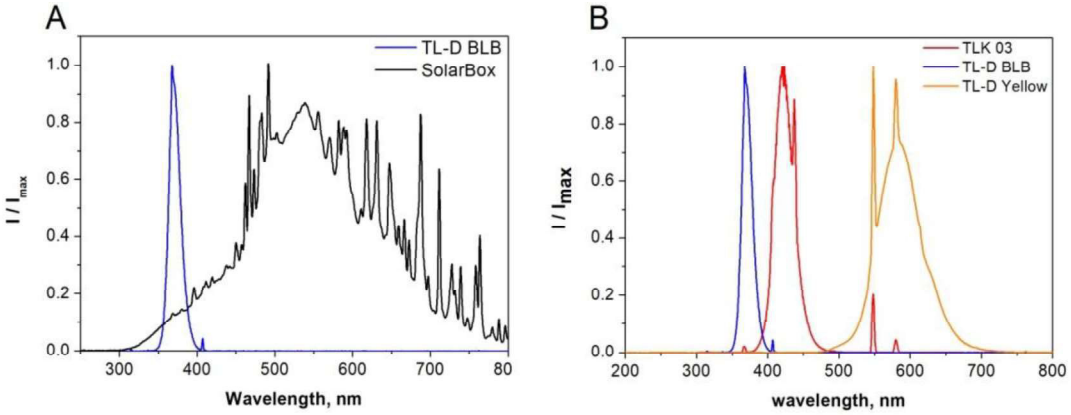

Fig. 1. Emission spectra normalized to the maximum intensity peak for the lamps used during the photocatalytic degradation experiments of (A) 2,4-DCP and (B) 1-naphthol.

The emission spectra of used irradiation sources were recorded through an Ocean Optics USB2000+UV-VIS equipped with a 400 μm optical fiber (30 cm length) with a cosine corrector (Ocean Optics, CC-3-UV-T, optical diffuser in PTFE, wavelength range 200-2500 nm, OD diameter 6.35 mm, Field of View 180°). Three different irradiation conditions were adopted: *i*) a set of three Philips TL-D 18 W BLB fluorescence lamp for UV only irradiation; *ii*) a sun simulator (SOLARBOX, CO.FO.ME.GRA., Italy) with λ≤340 nm cut-off filter for UV+Vis irradiation and *iii*) the same sun simulator, but with a λ≤420 nm cut-off filter for Vis only irradiation. The emission spectra of the irradiation sources are reported in Fig. 1A. The additional experiments with 1-naphthol were carried out with three different irradiation sources: *i*) Philips TL-D 18 W BLB fluorescence lamps (the same used for 2,4-DCP) for UV-only; *ii*) Philips TLK 03 fluorescence lamps for UV+Vis and *iii*) Philips TL-D 18 W yellow for Vis-only. Fig. 1B shows the emission spectra of the lamps used for the additional experiments with 1-naphthol. The measured light irradiance on the cell from 295-400 nm was

22 W m^{-2}, 28 W m^{-2} and 1.5 W m^{-2} for the Philips TL-D 18 W BLB fluorescence lamp, the SOLARBOX sun simulator, and the Philips TLK 03, respectively. For the Vis we are unable to measure the irradiance.

3 Results and Discussion

3.1 Photocatalytic transformation of 2,4-DCP

The transformation under UV irradiated TiO_2 of chlorophenols has been reported to produce more oxidized species (such as chlorobenzendiols, chloroquinones…)[28] and less chlorinated or condensation species through reductive pathways activated by the electron transfer of e_{cb}^- to the substrate and subsequent release of chloride ion in solution.[29] 2,4-DCP represents in this light an ideal substrates to test the photocatalytic properties of the TiO_2-rGO.

The photocatalytic degradations of 2,4-DCP at different initial concentration (C_0 from 5×10^{-5} to 1×10^{-3} M) were carried out on both 0.5 and 10%rGO(*HTR*)-N100 under UV only irradiation (Philips 18W BLB lamp). The time profiles in dark (adsorption) and under irradiation (photocatalytic degradation) are reported in Fig. 3-SM and Fig.4-SM. At the end of the equilibration time in dark (at least 2 hours) the concentration of 2,4-DCP in solution was stable. From the difference between the nominal concentration and the concentration in dark at the equilibrium the adsorption isotherm of 2,4-DCP on the two catalysts (Fig. 2A) is obtained. From the comparison between the two adsorption profiles at low and high rGO loading it is manifest that *i*) 2,4-DCP is mainly partitioned on the rGO phase being the amount of 2,4-DCP adsorbed on 10%rGO catalyst more than 3 times that adsorbed on the 0.5%rGO one (at the same concentration of free 2,4-DCP); *ii*) in both cases the empirical Freundlich isotherm $C_{bound} = K_{ads} \times C_{free}^{n}$ well describes the data. This isotherm is usually observed in the case of a marked heterogeneity of the adsorbing surface sites, in line with the hybrid nature of the investigated catalysts. From the fitting of the experimental profiles, n=0.83±0.06 and n= 0.45±0.02 were obtained for the catalyst with 0.5% and 10% of rGO, respectively, in agreement with the more complex nature of the adsorption sites in the catalyst with the highest rGO loading.

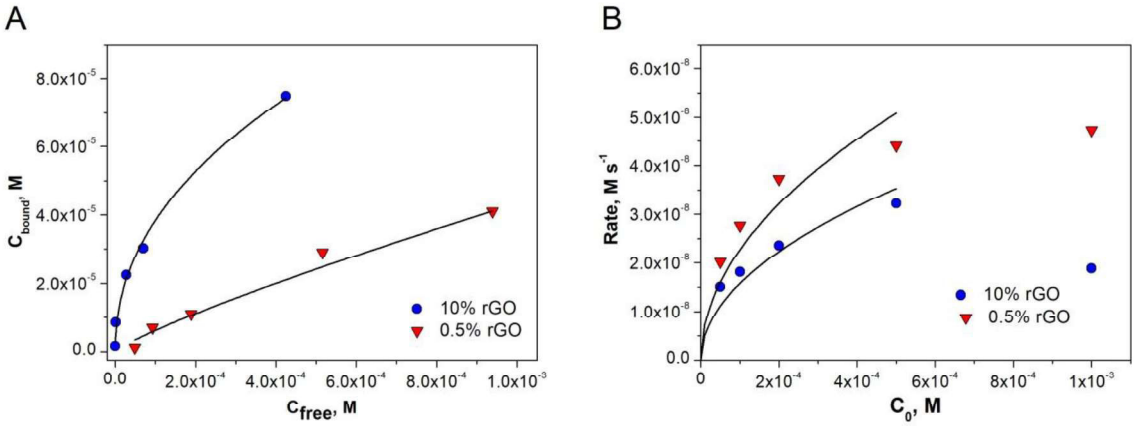

Fig. 2. (A) Adsorption isotherm of 2,4-DCP on 0.5% and 10%rGO(*HTR*)-N100; (B) Photocatalytic degradation rate of 2,4-DCP on 0.5 % and 10%rGO(*HTR*)-N100 (pH 3, C_{cat} = 500 mg dm^{-3}, UV only irradiation source) as a function of the initial concentration (C_0). The continuous lines in Fig. B show the fit according to a square root dependence of the rate from C_0 (reaction order =0.5).

The Fig. 2B shows the initial degradation rates measured as a function of the initial 2,4-DCP concentration. The transformation rate at low C_0 followed the 0.5 order of reaction often observed [18,30,31]. At larger C_0 the order n=0 was observed for 0.5% rGO. This agrees with the standard kinetic model.[30,32] The bell-shaped profile observed at 10%rGO loading can be interpreted in the light of the increment of the kinetic of recombination at high C_0 as a consequence of the increased concentration of 2,4-DCP at the surface of the catalyst, which can favor recombination processes mediated by adsorbed species (*back reactions*).[33] Presumably, 2,4-DCP can be oxidized by h_{vb}^+ and later reduced by e_{cb}^- acting as an efficient recombination center. A similar behavior was previously reported for glycerol under similar photocatalytic conditions.[34,35] The different behavior between the two loading conditions can be interpreted in the light of their different ability to adsorb 2,4-DCP. The 10%rGO catalyst is a better adsorbent for the substrate and consequently it adsorbs an amount of 2,4-DCP larger than that on the 0.5%rGO. This can promote the recombination process mediated by the adsorbed substrate. The lower rate observed with the largest loading of rGO suggests also that rGO could favor the recombination of charge carriers (both h_{vb}^+ and e_{cb}^-) photo-produced in one of the two phases or in both, in addition to the shielding of the TiO_2 phase.

To minimize the recombination reaction mediated by the substrate, we fixed 2,4-DCP 2×10^{-4} M, for which the reaction order is still n≈0.5 (see Fig. 2B), as observed in experiments with pristine TiO_2.[32]

3.1.1 Different irradiation sources

The degradation of 2,4-DCP 2×10^{-4} M on TiO_2-rGO hybrids with increasing loading of rGO (from 0 to 20%) under UV-only irradiation was investigated. For the overall profiles of adsorption (in the dark) and subsequent photocatalytic degradation refer to Fig. 5SM. The first order kinetic constants for the photocatalytic degradation are reported in Fig. 3 (black bars). Alongside the increment of the rGO loading a decrease of the transformation rate was observed. The decrease is less marked at large rGO loadings (≥ 4%) in the case of N100 (Fig.3A).

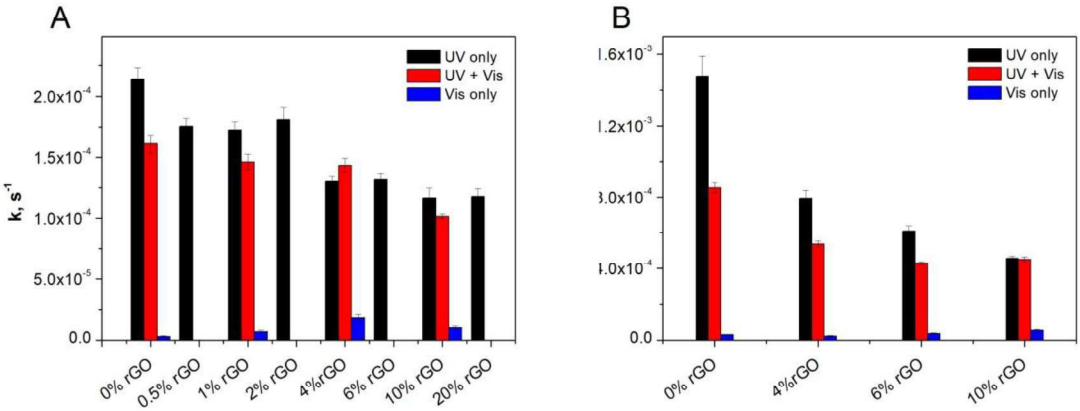

Fig. 3. Photocatalytic degradation of 2,4-DCP on (A) N100- and (B) P25-hybrids with different rGO loadings under UV only, UV + Vis (λ ≥ 340 nm) and Vis only (λ ≥ 420 nm). Conditions: pH 3, C_{cat} = 500 mg dm^{-3}, $C_0 = 2\times10^{-4}$ M.

However, the amount of 2,4-DCP adsorbed increases with the overall amount of rGO. Fig.4 reports the fraction of adsorbed 2,4-DCP, C_{bound}/C_0, where C_0 is the total 2,4-DCP

concentration added to the system. At rGO% loading higher than 2% a monotonic increment of the 2,4-DCP bound at the catalyst surface as a function of the overall amount of carbonaceous phase was observed.

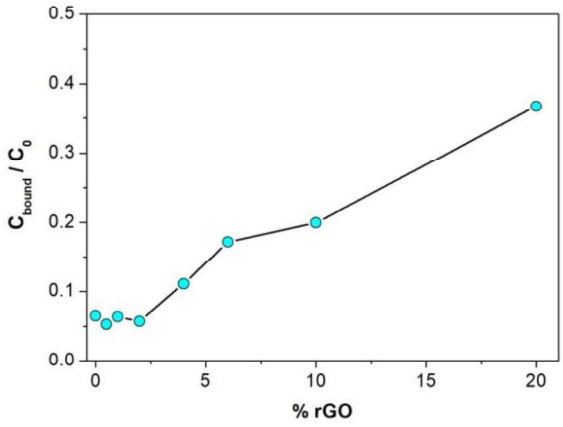

Fig. 4. Fraction of 2,4-DCP adsorbed on N100-hybrids as a function of the %rGO loading (conditions: $C_0 = 2\times10^{-4}$ M, pH 3, C_{cat} = 500 mg dm^{-3}, $C_{bound} = C_0 - C_{free}$).

The decrease of the kinetic constants with %rGO can be partially interpreted in the light of a shielding effect of the carbonaceous phase for the UV photons able to activate the photocatalytic process on TiO_2. However, an increment of back reactions at higher rGO loading cannot be excluded (see above). Even in this case the trend for the photocatalytic rate with a plateau at rGO≥ 4% cannot be totally interpreted in this light, because the amount of bound 2,4-DCP is linearly correlated with the rGO loading. To partially compensate both the shielding effect and the increment of the recombination rate (mediated by the adsorbed 2,4-DCP), a different reason that would favor the 2,4-DCP transformation at high rGO% has to be invoked. At this stage it is only possible to suppose either a partial activity of rGO itself under UV-only irradiation or an increment of the photogenerated charge separation.[36,37,38]

A possible photocatalytic mechanism involving rGO absorption was checked with broad band irradiation. The 2,4-DCP transformation on catalysts with different rGO% loading (*n*%rGO(*HTR*)-N100 with *n* = 0, 1, 4, 10%) was studied under UV+Vis irradiation obtained through a sun simulator with a cut off filter able to block λ≤340 nm. The related kinetic constants are reported in Fig. 3A (red bars). Even in this case a decrement of the overall transformation rate was observed with the increase of the rGO loading, but it is lower than in the case of UV-only irradiation. It emerges that, although rGO does not have a positive effect on the overall photocatalytic, rGO activates some minor processes able to compensate partially for its shielding effect of TiO_2.

The first order kinetic constants on the same catalysts (*n*%rGO(*HTR*)-N100 with *n* = 0, 1, 4, 10%) under Vis-only irradiation (λ≥420 nm, with a cutoff filter on SOLARBOX) are reported in Fig. 3A (blue bars). For Vis irradiation the rate is dramatically lower than under UV, but not null. A slight increment of the 2,4-DCP degradation rate was observed with the increment of the rGO%. A small Vis activity of rGO, that implies also a small UV activity, could be one of the reasons previously invoked that are able to compensate the decrement in the photocatalytic rate observed under UV-Vis irradiation.

3.1.2 Activity of hybrids with different TiO_2

With the aim to clarify if the nature of the TiO_2 affects the photocatalytic mechanism, rGO-TiO_2 hybrids with P25 were synthesized (*n*%rGO(*HTR*)-P25 with *n* = 0, 1, 4, 10%). The photocatalytic activity of these catalysts was compared toward 2,4-DCP degradation in the same conditions adopted in the previous experiments ($C_0 = 2\times10^{-4}$ M, pH 3, C_{cat} = 500 mg dm^{-3}) under the same irradiation sources (UV-only, UV+Vis and Vis-only).

Fig. 5 shows all the experiments carried out with *n*%rGO(*HTR*)-P25: the columns report the different irradiation systems (UV-only, Vis-only and UV+Vis, respectively) and the rows the different rGO loading (from 0 to 10 %). Fig. 3B reports the related kinetic constants.

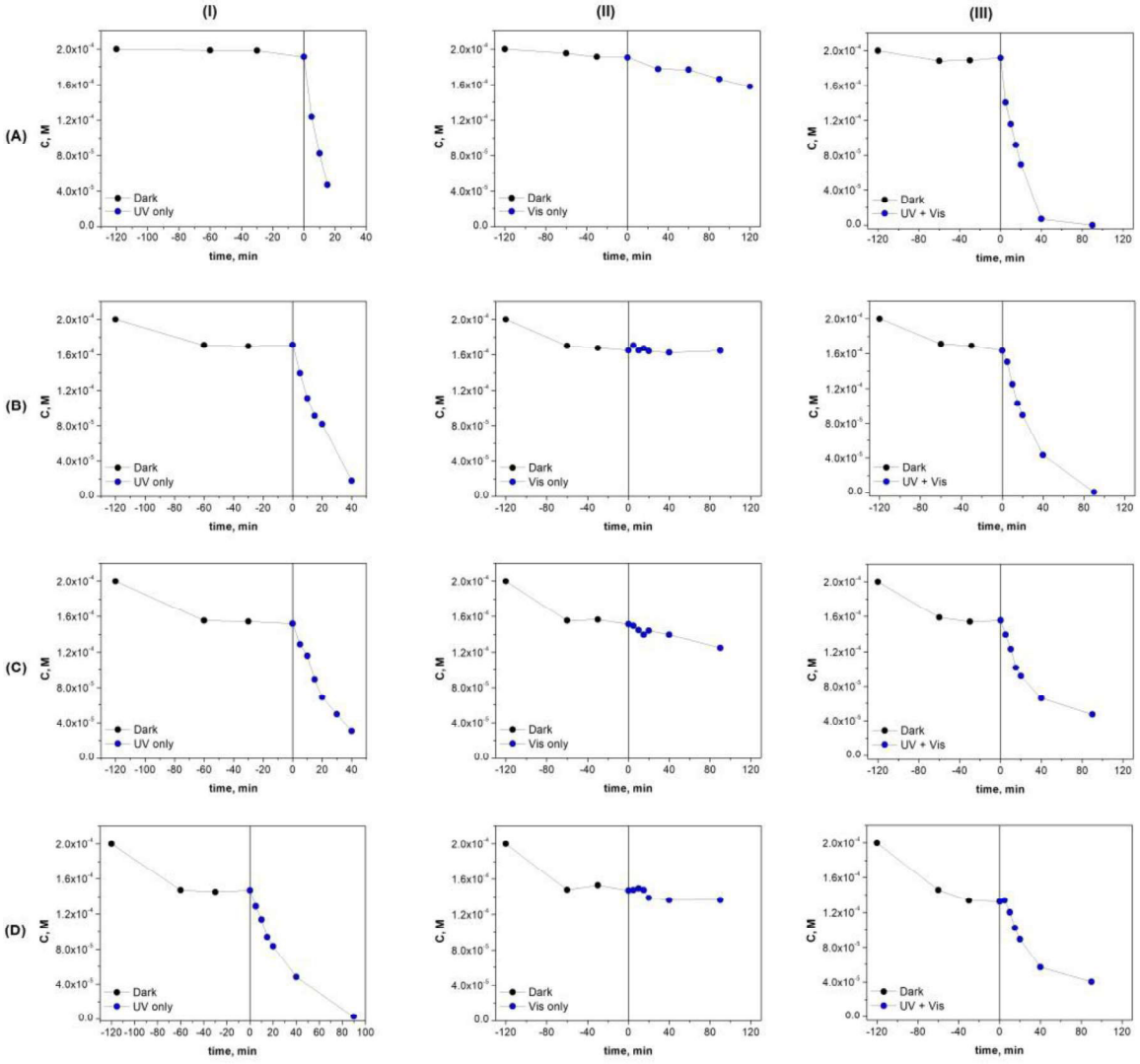

Fig. 5. Adsorption (dark) and photocatalytic degradation (light) of 2,4-DCP on P25 hybrids with different %rGO loadings: (A) 0%, (B) 4%, (C) 6% and (D) 10% and under different irradiation conditions: (I) UV-only, (II) Vis only (λ ≥ 420 nm) and (III) UV + Vis (λ ≥ 340 nm). Conditions: $C_0 = 2\times10^{-4}$ M, pH 3, C_{cat} = 500 mg dm^{-3}.

The analysis of all these data and the comparison with the kinetic data measured with N100, suggest:

i) In the presence of UV irradiation (UV-only or UV-Vis) the photocatalytic transformation of 2,4-DCP is faster on the pristine P25 than on N100. The ratio between the two kinetic constants on the bare catalysts and under UV-only is $\frac{k_{obs}^{P25}}{k_{obs}^{N100}} = 6.9 \pm 0.8$. A marked dependence of the rate for different substrates from the nature of TiO_2 was previously reported, and a marked selectivity toward specific substrates or classes of substrates emphasized.[39]

ii) The effect of the rGO on the kinetics of transformation of 2,4-DCP is the same both for the N100-based and TiO_2-P25-based catalysts. With the increment of rGO the photoactivity of the catalysts decreases, and the relative decrement is lower under UV+Vis irradiation than under UV-only source. A limited Vis activity was also observed and, as previously observed, this activity increases shlightly with the increment of the rGO loading.

iii) The depressing role of rGO on the photocatalytic activity under UV-only is more marked in the P25-based catalysts with respect to N100. Note that the ratio between the kinetic constants observed under Vis-only on 10%rGO(*HTR*)-P25 and 10%rGO(*HTR*)-TiO_2 100 is 3.9±0.4, significantly lower than the ratio reported at point i) for the pristine catalysts. The negative effect due to the rGO phase on the overall photocatalytic activity under UV irradiation is strongly related not only to the nature of the carbonaceous phase synthesized, but also to the type of TiO_2 employed. This outlines the importance of the size of TiO_2 particles, for scattering effects, and of the surface texture, that in the synthetic process produces a different coupling between the two phases.

3.2 Adsorption evaluation

In the composite catalyst there are two distinct phases (rGO and TiO_2) that concurrently adsorb the analyte. Let fix rGO phase as phase #1, and TiO_2 as phase #2. The adsorption constant for each phase can be expressed as $K_i^{ads}=[A_{b,i}]/([S_i][A_w])$, corresponding to the reaction $a_w + s_i = a_{b,i}$, where $[A_{b,i}]$ is the concentration of analyte bound to the adsorber i, $[S_i]$ the concentration of free adsorbing sites s_i, and $[A_w]$ the concentration of the analyte in the water solution. Considering that adsorption on the two different phases is not competitive, for each phase the number balance of sites, $C_{s,i}=[S_i]+[A_{b,i}]$, is worth. Then $[A_{b,i}]=C_{s,i} K_i^{ads}[A_w]/(1+ K_i^{ads}[A_w])$. In the approximation of low surface coverage, this can be linearized as $[A_{b,i}]= C_{s,i} K_i^{ads}[A_w]$, and then considering two phases the total amount of adsorbed analyte $[A_b]= [A_w](C_{s,1} K_1^{ads}+ C_{s,2} K_2^{ads})$.

For experiments in which the concentration of the hybrid catalyst $C_{cat} =M_{cat}/V$ [g L^{-1}] is constant, the adsorbing sites concentration $[C_{s,i}]$ is easily expressed as $[C_{s,i}]=\varphi_i C_{cat} \sigma_i$, where φ_i is the mass fraction of phase i on the composite catalyst and σ_i is the density of adsorbing sites [n_{sites} g^{-1}] of phase i. Considering that the fraction adsorbed onto the hybrid catalyst is $f_{ads}=[A_b]/[A_{tot}]$, it can be easily shown that $[A_b]/[A_w]= f_{ads}/(1- f_{ads})$.

For a hybrid catalyst with two adsorbing phases, one obtains:

$$\frac{f_{ads}}{1-f_{ads}} = K_2 + (K_1 - K_2)\varphi \qquad \text{(eq. 1)}$$

where the adimensional constant $K_i= C_{cat} \sigma_i K_i^{ads}$ at constant C_{cat} and σ_i is proportional to K_i^{ads} [M^{-1}], and where φ refers to the fraction of rGO in the composite catalyst, subscripts (1) and (2) to rGO and TiO_2, respectively. As $f_{ads}= 1-C/C_o$ is experimentally known from the experimental concentration C in the aqueous phase after adsorption, the above linear

relationship between $f_{ads}/(1-f_{ads})$ versus φ allows to estimate K_1 and K_2, and then to assess where the substrate is preferentially adsorbed.

Fig. 6 shows the plot according to eq.(1) of all adsorption data collected at different %rGO for N100 and P25 based hybrids. The values of K_1 and K_2 obtained under different irradiation conditions are reported in Table 1 (see later for a discussion).

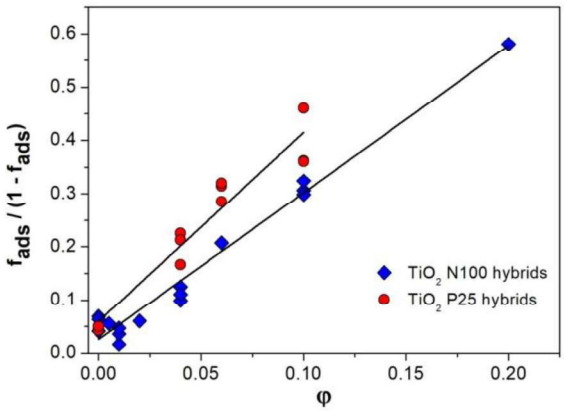

Fig. 6. Fit according to eq. 1 of the adsorption experimental data for N100- and P25-hybrids.

3.3 Kinetic model to decouple the photocatalytic activity of the two phases

Here we develop for the first time a two-phase kinetic model for a hybrid photocatalyst, which is applicable when both phases or only one absorbs light. Here we follow the same treatment already developed for kinetic in photocatalytic systems,[32] as the model was validated several times [30,31]. Each material is considered separately for light absorption, the recombination reaction and reactivity with the oxidant (O_2) and the analyte, and their contribution to the overall rate is proportional to their mass fraction in the catalyst, as done above for the analysis of adsorption. However, as the produced charge carrier after light absorption in each material are supposed to exchange between the two phases of the hybrid catalyst, to approach this issue we consider the total amount of formed holes (or total excited electrons), and assume that a fast equilibrium is reached between the two phases regulated by an equilibrium constant $K_h=[h_{eq,1}]/[h_{eq,2}]$ and $K_e=[e_{eq,1}]/[e_{eq,2}]$, respectively for holes and electrons. For example, holes produced on TiO_2 VB can migrate to rGO, adding to that possibly formed on rGO itself after light absorption, the electrons can migrate from rGO to TiO_2, adding to that formed on TiO_2, or the reverse, or any combination of them. Then $[h_{eq,1}]=\beta_h[h_{tot}]$, $[h_{eq,2}]=(1-\beta_h)\,[h_{tot}]$, and $[e_{eq,1}]=\beta_e[e_{tot}]$, $[e_{eq,2}]=(1-\beta_e)\,[e_{tot}]$ where the fraction $\beta_i = K_i/(1+K_i)$ and $[h_{tot}]$ and $[e_{tot}]$ are the sum of holes and excited electrons, respectively, produced by the independent absorption of the two materials in the hybrid catalyst. Then the actual concentration of reacting species produced by light absorption of the hybrid catalyst ψ_h and equilibrated between the two phases is $[h_{eq,1}]= \beta_h\,\psi_h$ and $[h_{eq,2}]= (1-\beta_h)\,\psi_h$. The same is worth for electrons in the upper energy level. Only in the case that the two materials have not a strong electronic coupling, the absorption $\psi_h =(\psi_{1+}\psi_2)$, where ψ_i is the absorbed photon flux by each material *i*. Because the amount of absorbed light is proportional to ε_i, the extinction coefficient of the pure phase *i,* and ψ_o, the incident light intensity, then $\psi_i = b\,\varepsilon_i\,\psi_o\,\varphi_i\,C_{cat}$, where ε_i is the absorption coefficient [g^{-1}] and *b* the slurry thickness used in the experiments.

For practical convenience, $(\psi_{1+}\psi_2) = [\omega_1 \varphi + \omega_2 (1-\varphi)]$, where $\omega_i = b\ \varepsilon_i\ \psi_o\ C_{cat}$ are constant if ψ_o and C_{cat} are constant for the set of experimental data.

With the above assumptions a steady state approximation is applied to the rate equations for $d[e_{tot}]/dt$ and $d[h_{tot}]/dt$ considering the generation rate $(\psi_{1+}\psi_2)$, and in each material the recombination of charge carriers, the reaction of excited electrons with oxygen and that of holes with the adsorbed substrate. The solution for the quantum yield ($QY=rate/\psi_h$) is here developed only for the oxidative side (oxidation by holes) of the photocatalytic process, for sake of simplicity. The solution is identical to that already reported [30], i.e. $QY = -y + \sqrt{y(y+2)}$), but with a different expression for the master variable y (here omitted). Under the approximation that y<<1, that is a QY<0.20 and definitely at low C_0, $QY = \sqrt{2y}$, and then the rate is

$$rate = \sqrt{k_{cat}[A_{tot}]} = \sqrt{k_1[A_{b,1}] + k_2[A_{b,2}]}\sqrt{\psi_h} \qquad \text{(eq. 2)}$$

The square root dependence on $[A_{tot}]=C_o$ is already evident in Fig. 2B, provided that C_0 is small as in the experiments here analyzed. Using the relationships derived above in the analysis of adsorption for $[A_{b,i}]$ and for ψ_h (under the linear combination hypothesis), the rate constant k_{cat} in the hybrid catalyst is

$$k_{cat} = \frac{[k_1K_1\varphi + k_2K_2(1-\varphi)][\omega_1\varphi + \omega_2(1-\varphi)]}{1 + K_1\varphi + K_2(1-\varphi)} \qquad \text{(eq. 3)}$$

where $k_1 = k_{red,T}\ [O_2]\ \beta_h\ k_{ox,1}$, $k_2 = k_{red,T}\ [O_2]\ (1-\beta_h)\ k_{ox,2}$, $k_{red,T}$ is the composite rate constant of reaction of excited electrons with O_2 equal to $k_{red,T} = (\beta_e\ k_{red,1} + (1-\beta_e)\ k_{red,2})/(\beta_e\ \beta_h\ k_{R,1} + (1-\beta_e)(1-\beta_h)\ k_{R,2})$, in which $k_{R,i}$ are the recombination rate constants of charge carriers, and $k_{ox,i}$ and $k_{red,i}$ are the reaction rate constants for oxidation of the substrate by holes and reduction of O_2 in the two phases, respectively. The significance of K_1 and K_2 ($K_i = C_{cat}\ \sigma_i\ K_i^{ads}$) and $\omega_i = b\ \varepsilon_i\ \psi_o\ C_{cat}$ have been above reported.

This is the main result for the two-phase photocatalytic model, where the adsorption/desorption rate is regulated by the adsorption equilibrium constants $K_{i=1,2}$ on the two phases, the fraction φ of rGO and the fraction $(1-\varphi)$ of TiO_2 in the composite catalyst, which is used in the experiments at constant and fixed concentration C_{cat}. The kinetic composite constants k_1 and k_2 are constants at fixed [O_2] as done in the experiments. The dependence of k_{cat} on k_1, k_2, K_1, K_2, ω_1 and ω_2 is then quite complex and justifies the paper title about the complex interplay between adsorption and photoactivity in hybrids rGO/TiO_2. The equation shows that the $rate = k_{obs}\ C_o^{1/2}$ (see Fig. 2B) for low C_0 depends basically from the convolution of the square root of 3 terms: 1) the rate constants weighted with adsorption constants and relative mass fraction of each hybrid material constituent; 2) the optical properties of the two materials and used irradiation spectra; 3) the adsorption constants weighted with mass fraction of each hybrid material constituent. The model has a general application to whatever material the hybrid is formed of.

The kinetic model, although approximated for low quantum yields and linear adsorption, is able to foresee, in the case of this paper, if addition of rGO to TiO_2 is beneficial or not, and to decouple the effects of adsorption from intrinsic kinetic factors. Given that K_1 and K_2 can be independently measured (see eq. 1), the partition of charge carriers β_i, included in k_1 and k_2,

can be estimated although weighted by the actual true kinetic constants $k_{ox,i}$ (see the definition of these constants below eq. 3). As the ratio $k_1/k_2 = \beta_h\, k_{ox,1}/((1-\beta_h)\, k_{ox,2})$, and remembering that $\beta_h = K_h/(1+K_h)$, the ratio $k_1/k_2 = K_h\, k_{ox,1}/\, k_{ox,2}$ gives a direct information on the partition of holes and their reactivity in the two phases. The kinetic constants $k_{ox,i}$ reflect the probability of holes to react with the substrate, and their values depend on the position of energy levels, on which they are located, relative to the substrate redox potential. For example, if holes moves to graphene K_h would be large, but if the energy level where they move is more negative than the redox potential for oxidation of the substrate, $k_{ox,1}$ will be negligible, resulting in a negligible value of the ratio k_1/k_2.

In this kinetic model the effect of wavelength of illumination is also contemplated. In UV both TiO_2 and rGO can absorb. However under VIS irradiation, ω_2 is null. The assumption that absorption $\psi_h = (\psi_1 + \psi_2)$ is quite approximated, as it does not include possible synergic effects, including strong electron coupling between the materials and their mutual shading, which have been invoked before, and also already reported by our research group [19]. In the quoted paper it was shown that 5% rGO is able to decrease the extinction of the TiO_2 by 20% at 350 nm, probably reducing more the scattering than the absorption. However, the assumption has the merit to show the many dependences of light absorption from material's type and hybrid composition.

As the denominator in eq. 3 can be directly calculated from the experiment (see Fig. 6), eq. 3 can be transformed into:

$$\frac{k_{obs}^2}{1-f_{ads}} = [k_1 K_1 \varphi + k_2 K_2 (1-\varphi)][\omega_1 \varphi + \omega_2 (1-\varphi)] \qquad \text{(eq. 4)}$$

Eq. 4 forecasts that the experimental LHS term has a parabolic dependence on φ. The parabolic fit on experimental data $k^2_{obs}/(1-f_{ads}) = A\,\varphi^2 + B\,\varphi + C$ is reported for N100 and P25 in Fig. 7(inset). The fit is quite good. However, the constant terms A,B,C depend on 6 parameters of which 4 are unknown (actually k_1, k_2, ω_1, ω_2), and then it is not possible to get a value for them. The sole valuable value is the intercept, that corresponds to $k_2 \times K_2 \times \omega_2$ As K_2 is known from adsorption analysis, $k_2 \times \omega_2$ is evaluated and reported in Table 1.

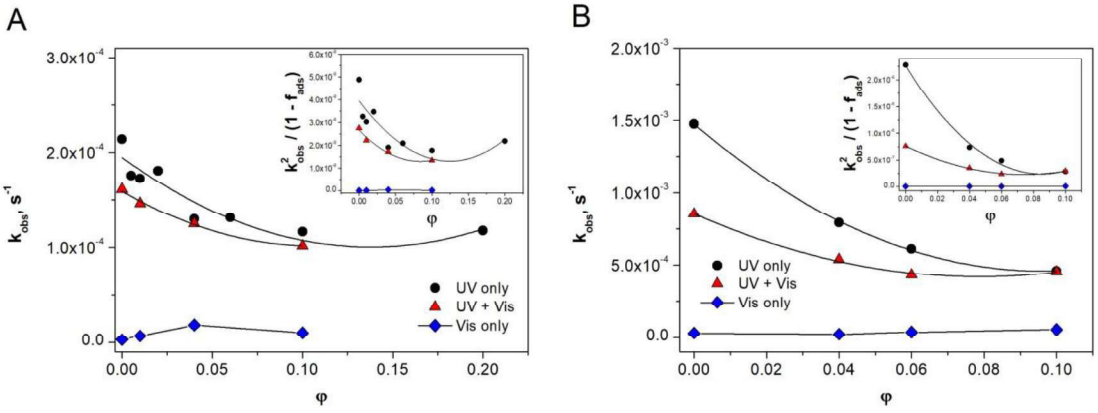

Fig. 7. Experimental k_{obs} as a function of the fraction φ of rGO on N100 (A) and P25 (B) hybrid catalyst. Insets: experimental $k^2_{obs}/(1-f_{ads})$ vs. φ. The solid lines are the quadratic fits according to eq. 4.

Alternatively, at low φ the experimental data can be approximated by a straight line. This follows from eq. 4 assuming that under UV irradiation, or UV+VIS irradiation, only TiO_2

absorbs light. This assumption is supported by the low reported extinction of rGO on SiO_2 [19] from which is apparent that the net extinction due to rGO is low at all wavelengths. Eq.4 is the convolution of two straight lines $z_1=k_2K_2+(k_1K_1-k_2K_2)\varphi$, and $z_2=\omega_2+(\omega_1-\omega_2)\varphi$. Accordingly, z_2 must have a negative slope. The increase of $k^2_{obs}/(1-f_{ads})$ at large rGO fractions can be claimed as a synergic effect of rGO. As the convolution of the two straight lines must increase at large φ, z_1 must have a positive slope. To obtain that at least at φ=1 the function value is equal to that at φ=0, the following condition must be satisfied: $k_1K_1/k_2K_2>\omega_2/\omega_1=\varepsilon_2/\varepsilon_1$. Then from Table 1 $k_1/k_2>9.3\times10^{-3}\varepsilon_2/\varepsilon_1$ and $k_1/k_2>1.7\times10^{-2}\ \varepsilon_2/\varepsilon_1$ for N100 and P25 hybrids, respectively. If these conditions are satisfied, the increase of $k^2_{obs}/(1-f_{ads})$ at large rGO fractions is possible. As the reported extinction of rGO on SiO_2 (see Fig.2 in [19]) at 360 nm is about 200, then $\varepsilon_2/\varepsilon_1\approx12000/200=60$ for N100. It follows for N100 that $k_1/k_2>0.56$. A similar condition is worth for P25 [40], for which the extinction coefficient at 365 nm $\varepsilon_2= 2.5\times10^4$ cm^2g^{-1}, i.e $\varepsilon_2/\varepsilon_1\approx25000/200=120$. Then $k_1/k_2>2.0$ for P25.

From the limit values $k_1/k_2>0.56$ and $k_1/k_2>2.0$ for N100 and P25, respectively, the rGO is beneficial only if the microscopic reactivity on rGO, $k_1=k_{red,T}$ $[O_2]$ β_h $k_{ox,1}$, is almost equal to that of TiO_2, $k_2=k_{red,T}$ $[O_2]$ $(1-\beta_h)$ $k_{ox,2}$. As $k_1/k_2 = K_h$ $k_{ox,1}/$ $k_{ox,2}$, to obtain the reported ratios $K_hk_{ox,1}\approx$ $k_{ox,2}$. Two limiting hypotheses are possible: 1) if on rGO the substrate oxidation is very efficient, a limited partition of holes on rGO can be compatible; 2) if the holes are quantitatively injected from TiO_2 to rGO, a limited catalytic role of rGO can be tolerated. All other cases are intermediates between the above.

As k_2 for P25 is larger than k_2 for N100 (about 3.6 times), the effect of rGO can be seen on P25 only at larger %rGO than those needed for N100 (compare Fig.7A with 7B). This conclusion is relevant as the beneficial effect of rGO in hybrid catalysts is evident only if the semiconductor is not particularly efficient.

Table 1. Adsorption and degradation constants obtained from the fitting of the degradation kinetic and adsorption data in the presence of the catalysts with different %rGO loading (left column: N100 hybrids; right column: P25 hybrids).

N100 hybrids	
Adsorption	
K_1	2.79 ± 0.12
K_2	0.026 ± 0.008
K_2/K_1	$(9.3\pm0.5)\times10^{-3}$
Photocatalytic degradation	
$k_2\omega_2$ (UV only)	$(5.5 \pm1.9) \times 10^{-3}$
$k_2\omega_2$ (UV+Vis)	$(3.7 \pm1.3) \times 10^{-3}$

P25 hybrids	
Adsorption	
K_1	3.61 ± 0.32
K_2	0.060 ± 0.019
K_2/K_1	$(1.7\pm0.5)\times10^{-2}$
Photocatalytic degradation	
$k_2\omega_2$ (UV only)	0.14 ± 0.04
$k_2\omega_2$ (UV+Vis)	$(4.6 \pm1.4) \times 10^{-2}$

The results obtained from the adsorption model and the reduced kinetic model (eq. 1 and 5) are summarized in Table 1 for N100- and P25-based catalysts (left and right column, respectively). The data include the type of irradiation source, except for Vis only. From the comparison between the adsorption and photocatalytic degradation constants obtained in the different experimental conditions, some further conclusions can be drawn:

i) The adsorption on P25 phase is roughly double with respect to that of the pristine N100. This justifies the larger activity of naked P25 with respect to naked N100 already discussed under paragraph 3.1.2 (see also Fig.4). In all hybrids the 2,4-DCP adsorption is completely unbalanced toward the rGO phase, with adsorption constant from 60 to 110 times higher for the rGO phase with respect to TiO_2.

ii) Under Vis-only irradiation a very low but not null activity is observed (see Fig.7). As the Vis activity is almost independent of the rGO fraction, this can be mostly attributed to the sensitization of interfacial states created by the coupling with rGO.

iii) The degradation kinetic constants related to the inorganic phase are significant higher for TiO_2-P25 than for N100, particularly under UV-only irradiation, but the decrement is significantly higher for P25-based materials than for N100-based catalysts. This implies a different electron coupling with rGO.

3.4 Photocatalytic transformation of 1-Naphthol

A different substrate was also checked to assess if previous conclusions are substrate-dependent. The substrate chosen was 1-naphthol because *i*) it is strongly adsorbed at the surface of the hybrid catalyst and *ii*) it cannot be degraded through a reductive pathway, as 2,4-DCP does.[29] The catalysts were obtained through the chemical reduction of GO as in [19] with the aim to test if the reductive procedure affects significantly the photoactivity of the catalyst. The results obtained on catalysts synthesized through the hydrothermal and chemical routes did not show significantly differences.

The photocatalytic transformation of 1-naphthol on 2%rGO*(CR)*-N100 at different substrate concentrations (from 2.5×10^{-5} to 5×10^{-4} M) were carried out under UV-only irradiation. From the raw experimental profiles in the dark and under irradiation (see Fig. 6SM) the adsorption isotherm (Fig. 8) and the photocatalytic degradation constants as a function of the initial concentration C_0 (inset of Fig. 8) were obtained. As for 2,4-DCP, the adsorption isotherm for 1-naphthol is well described by a Freundlich isotherm with n = 0.33±0.08. From the photocatalytic kinetic constants measured, the photocatalytic transformation rates were computed and reported as a function of C_0 in Fig. 6SM-(f). As for the 2,4-DCP, a bell-shaped behavior was observed suggesting a surface recombination process mediated by the adsorbed substrate.[32] With 1-naphthol the back reactions were kinetically important even at relatively low rGO loading because of the higher adsorption of 1-naphthol than 2,4-DCP on the catalyst surface.

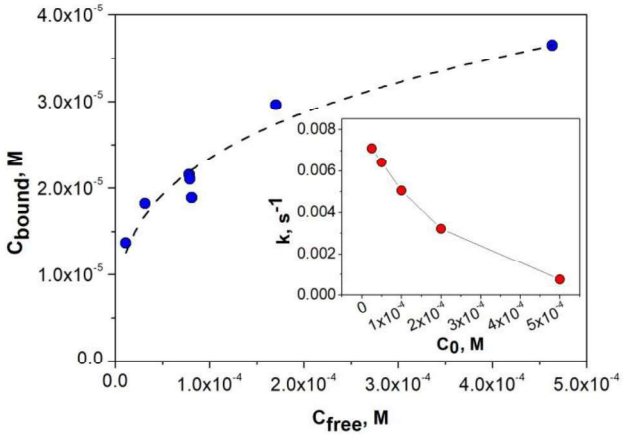

Fig. 8. Adsorption isotherm of 1-naphthol on N100 with 2%rGO*(CR)*. Inset: 1-naphthol photocatalytic degradation constant k_{obs} (pH 3, C_{cat} = 500 mg dm^{-3}, UV only) on 2%rGO*(CR)*-N100 at different initial concentration C_0.

The 1-naphthol photocatalytic degradation was explored under UV+Vis irradiation (see Fig. 1B) on catalysts with different rGO loading (*n*%rGO*(CR)*-N100 with *n* = 0, 2, 6 and 10 %). The raw profiles are reported in Fig. 7SM and the related kinetic constants summarized in Fig. 9. It is manifest that even in this case the rGO has a detrimental effect on the overall photocatalytic activity. The 1-naphthol photo-catalyzed transformation was tested also under Vis-only irradiation (yellow lamp, see Fig. 1B) on the same catalysts. The raw profiles are reported in Fig. 10, and the photocatalytic rate constants are also reported in Fig. 9. The Vis-only activity is quite low and the kinetic constants slightly increased with the rGO loading.

Interestingly, the analysis of the raw profiles in the dark shows that the adsorption of 1-naphthol on the TiO_2-rGO catalyst surface, especially at high rGO loading, is quite complex and apparently follows a double kinetic process in which 1-naphthol is fast adsorbed, probably on a family of adsorption sites easily reachable, and then the adsorption proceeds with lower rate, presumably on a family of less reachable sites (i.e. micro-porosity). This adds further difficulties for the interpretation of the data, because it is quite difficult to split the contribution of an effective degradation process from a progressive and slow adsorption. This could be a common drawback of the analysis of the transformation data obtained on highly heterogeneous adsorbing systems. This is not only the case of 1-naphthol (here reported), but also the case of the most used dyes employed to test the performance of innovative photocatalysts. In these cases the collection of robust experimental data useful to extract reliable conclusions on the photocatalytic activity is difficult and sometimes impossible. Additionally, data can be biased by large Vis irradiation intensity and improper UV cutoff that increase the modest activity of hybrid catalysts.

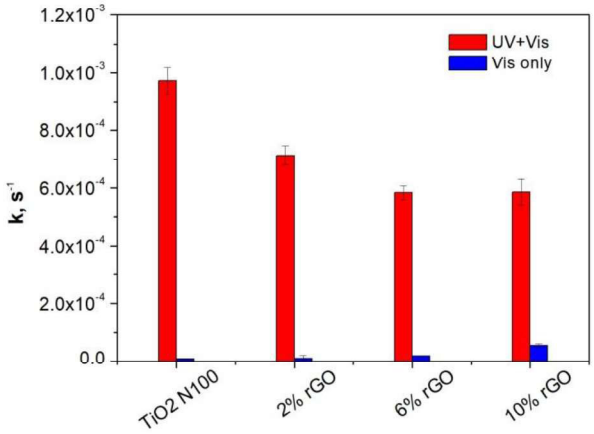

Fig.9. Degradation rate constants k_{obs} for 1-Naphthol on *n*%rGO*(CR)*-N100 (with *n*% equal to 0, 2, 6 and 10%) under UV+Vis and Vis only irradiation sources. Conditions: $C_0 = 1\times10^{-4}$ M, pH 3, C_{cat} = 500 mg dm^{-3}.

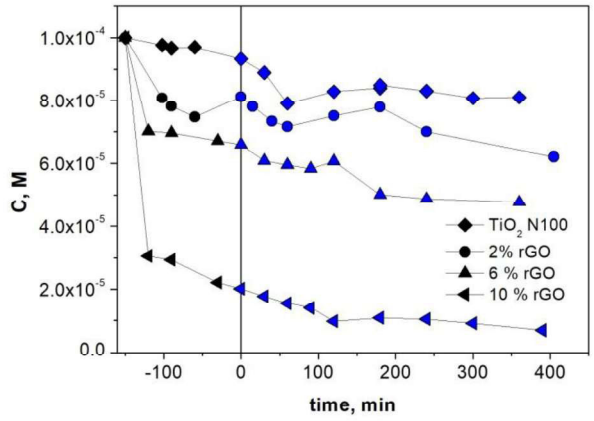

Fig. 10. Adsorption (dark) and photocatalytic degradation (Vis only irradiation) of 1-naphthol on N100-hybrids with different rGO loadings (%rGO*(CR)* = 0, 2, 6 and 10%) . Conditions: $C_0 = 1\times10^{-4}$ M, pH 3, C_{cat} = 500 mg dm^{-3}.

4 Conclusions

The acquired set of experimental data (different C_0, %rGO, type of TiO_2 and irradiation spectra) allowed a quantitative analysis of adsorption and kinetic parameters for the hybrid catalyst. The investigated substrates are adsorbed preferentially on the rGO and this gives an unbalanced phase partitioning of the organic substrate.

Significant degradation rates were observed only in the presence of UV irradiation. This suggests that the only photocatalytic mechanism operational is that based on the band-to-band transition promoted by the absorption of a UV photon from the semiconductor. The photogenerated carriers in the semiconductor hardly moves to the rGO phase where the substrate is mainly partitioned. Being the reductive pathway active during the 2,4-DCP photocatalytic transformation under pristine TiO_2, we can conclude that the photo-promoted electrons in the TiO_2 conduction band are difficulty injected in the rGO where the substrate is

mainly adsorbed. This is in agreement with our previous conclusion that the electron transfer process can occur from photoexcited states of rGO onto the titania, and holes can migrate from titania to rGO.[19]

The rGO phase did not give the hoped increment in the transformation rate of both 2,4-DCP and 1-naphtol, even if the inhibition effect caused by the presence of rGO was lower under UV-Vis because a not null visible activated degradation mechanism is operational.

The nature of the TiO_2 employed (N100 vs P25) does not influences significantly the overall photoactivity of the catalysts.

According to the discussion at paragraph 3.3, if the holes are quantitatively injected from TiO_2 to rGO, a limited catalytic role of rGO can be tolerated. However, since also in UV the rate is depressed, the holes in the rGO phase are not sufficiently oxidizing to promote the transfer of an electron from the HOMO of the adsorbed substrate (both 2,4-DCP and 1-naphthol) to the empty state of rGO. In other terms, the redox potential of the hole in the rGO (h^{+}_{rGO}) is not sufficiently high (low in energy) to promote the electron transfer from the HOMO of the adsorbed substrate to the empty state of rGO. Alternatively, if the photogenerated holes are efficiently transferred to the rGO phase, this acts as a recombination center. Furthermore, at high concentration the adsorbed substrate (both 2,4-DCP and 1-naphthol) can promote substrate mediated recombination processes.

The kinetic model here developed permits enucleation of some key factors influencing the photocatalytic rate. The model has a general validity and can be applied to binary photocatalysts whatever the nature of the phases is (e.g. inorganic/inorganic hybrids, carbon doped semiconductors). However, a more refined model on the dependence of light absorption by hybrid catalyst is desirable.

4.1 Acknowledgements

The authors are kindly grateful for the financial support to Università di Torino – (Ricerca Locale). MM acknowledges financial support from Marie Skłodowska-Curie Action – 765860 – AQUALITY – H2020-MSCA-ITN-2017.

Captions to Figures and Tables

Fig.1. Emission spectra normalized to the maximum intensity peak for the lamps used during the photocatalytic degradation experiments of (A) 2,4-DCP and (B) 1-naphthol.

Fig. 2. (A) Adsorption isotherm of 2,4-DCP on 0.5% and 10%rGO(*HTR*)-N100; (B) Photocatalytic degradation rate of 2,4-DCP on 0.5 % and 10%rGO(*HTR*)-N100 (pH 3, C_{cat} = 500 mg dm^{-3}, UV only irradiation source) as a function of the initial concentration (C_0); (C) 2,4-DCP bound as a function of the %rGO loading. The continuous lines in Fig. B show the fit according to a square root dependence of the rate from C_0 (reaction order =0.5).

Fig. 3. Photocatalytic degradation of 2,4-DCP on (A) N100- and (B) P25-hybrids with different rGO loadings under UV only, UV + Vis ($\lambda \geq 340$ nm) and Vis only ($\lambda \geq 420$ nm). Conditions: pH 3, C_{cat} = 500 mg dm^{-3}, $C_0 = 2\times10^{-4}$ M.

Fig. 4. Fraction of 2,4-DCP adsorbed on N100-hybrids as a function of the %rGO loading (conditions: $C_0 = 2\times10^{-4}$ M, pH 3, C_{cat} = 500 mg dm^{-3}, $C_{bound} = C_0 - C_{free}$).

Fig. 5. Adsorption (dark) and photocatalytic degradation (light) of 2,4-DCP on P25 hybrids with different %rGO loadings: (A) 0%, (B) 4%, (C) 6% and (D) 10% and under different irradiation conditions: (I) UV-only, (II) Vis only ($\lambda \geq 420$ nm) and (III) UV + Vis ($\lambda \geq 340$ nm). Conditions: $C_0 = 2\times10^{-4}$ M, pH 3, C_{cat} = 500 mg dm^{-3}.

Fig. 6. Fit according to eq. 1 of the adsorption experimental data for N100- and P25-hybrids.

Fig. 7. Experimental k_{obs} as a function of the fraction φ of rGO on N100 (A) and P25 (B) hybrid catalyst. Insets: experimental $k^2_{obs}/(1-f_{ads})$ vs. φ. The solid lines are the quadratic fits according to eq. 4.

Fig. 8. Adsorption isotherm of 1-naphthol on N100 with 2%rGO*(CR)*. Inset: 1-naphthol photocatalytic degradation constant k_{obs} (pH 3, C_{cat} = 500 mg dm^{-3}, UV only) on 2%rGO*(CR)*-N100 at different initial concentration C_0.

Fig.9. Degradation rate constants k_{obs} for 1-Naphthol on *n*%rGO*(CR)*-N100 (with *n*% equal to 0, 2, 6 and 10%) under UV+Vis and Vis only irradiation sources. Conditions: $C_0 = 1\times10^{-4}$ M, pH 3, C_{cat} = 500 mg dm^{-3}.

Fig. 10. Adsorption (dark) and photocatalytic degradation (Vis only irradiation) of 1-naphthol on N100-hybrids with different rGO loadings (%rGO*(CR)* = 0, 2, 6 and 10%) . Conditions: $C_0 = 1\times10^{-4}$ M, pH 3, C_{cat} = 500 mg dm^{-3}.

Table 1. Adsorption and degradation constants obtained from the fitting of the degradation kinetic and adsorption data in the presence of the catalysts with different %rGO loading (left column: N100 hybrids; right column: P25 hybrids).

645 **References**

[1] M. Minella, D. Fabbri, P. Calza, C. Minero, Current Opinion in Green and Sustainable Chemistry 6 (2017) 11-17.

[2] H. Yu, P. Xiao, J. Tian, F. Wang, J. Yu, ACS Appl. Mater. Interfaces 8 (2016) 29470-29477.

[3] M. Faraldos, A. Bahamonde, Catal. Today 285 (2017) 13-28.

[4] X. Li, R. Shen, S. Ma, X. Chen, J. Xie, Appl. Surf. Sci. 430 (2018) 53-107.

[5] X. Li, J. Yu, S. Wageh, A. A. Al-Ghamdi, J. Xie, Small 12 (2016) 6640-6696.

[6] F. Sordello, E. Odorici, K. Hu, C. Minero, M. Cerruti, P. Calza, Nanoscale 8 (2016) 3407-3415.

[7] Q. Huang, S. Tian, D. Zeng, X. Wang, W. Song, Y. Li, W. Xiao, C. Xie, ACS Catal. 3 (2013) 1477-1485.

[8] Q. Lang, Y. Chen, T. Huang, L. Yang, S. Zhong, L. Wu, J. Chen, S. Bai, Appl. Catal. B-Environ. 220 (2018) 182-190.

[9] Y. Xu, Y. Li, P. Wang, X. Wang, H. Yu, Appl. Surf. Sci. 420 (2018) 176-183.

[10] Q. Xiang, J. Yu, M. Jaroniec, J. Am. Chem. Soc. 134 (2012) 6575-6578.

[11] M. Hamandia, G. Berhault, C. Guillard, H. Kochkar, Molecular Catalysis 432 (2017) 125-130

[12] X. Yang, J. Qin, Y. Jiang, R. Li, Y. Li, H. Tang, RSC Adv., 2014, 4, 18627-18636.

[13] M. Nasr, S. Balme, C. Eid, R. Habchi, P. Miele, M. Bechelany, J. Phys. Chem. C 121 (2017) 261-269.

[14] A.W. Morawski,, E. Kusiak-Nejman, A. Wanag, J. Kapica-Kozar, R.J. Wróbel,B. Ohtani, M. Aksienionek, L. Lipińska Catal Today, 2017, 280, 108-113.

[15] M. Minella, M. Demontis, M. Sarro, F. Sordello, P. Calza, C. Minero, J. Mater. Sci. 50 (2015) 2399-2409.

[16] J.G. Radich, A.L. Krenselewski, J. Zhu, P.V. Kamat, Chem. Mater. 26 (2014) 4662-4668.

[17] L. Gu, J. Wang, H. Cheng, Y. Zhao, L. Liu, X. Han, ACS Appl. Mater. Interfaces 5 (2013) 3085-3093.

[18] V. Maurino, M. Minella, F. Sordello, C. Minero, Appl. Catal. A-Gen. 521 (2016) 57-67.

[19] M. Minella, F. Sordello, C. Minero, Catal. Today 281 (2017) 29-37.

[20] W.S. Hummers, R.E. Offeman, J. Am. Chem. Soc. 80 (1958) 1339.

[21] N.M. Huang, H.N. Lim, C.H. Chia, M.A. Yarmo, M.R. Muhamad, Int. J. Nanomed. 6 (2011) 3443-3448.

[22] M. Minella, D. Versaci, S. Casino, F. Di Lupo, C. Minero, A. Battiato, N. Penazzi, S. Bodoardo, Electrochim. Acta 230 (2017) 132-140.

[23] Q. Mei, K. Zhang, G. Guan, B. Liu, S. Wang, Z. Zhang, Chem. Commun. 46 (2010) 7319-7321.

[24] D. Li, M.B. Mueller, S. Gilje, R.B. Kaner, G.G. Wallace, Nat. Nanotechnol. 3 (2008) 101-105.

[25] C. Nethravathi, M. Rajamathi, Carbon 46 (2008) 1994-1998.

[26] Y. Zhou, Q. Bao, L.A.L. Tang, Y. Zhong, K.P. Loh, Chem. Mater. 21 (2009) 2950-2956.

[27] W. Fan, Q. Lai, Q. Zhang, Y. Wang, J. Phys. Chem. C 115 (2011) 10694-10701.

[28] J.-C. D'Oliveira, C. Minero, E. Pelizzetti, P. Pichat, J. Photochem. Photobiol. A-Chem. 72 (1993) 261-267.

[29] C. Minero, E. Pelizzetti, P. Pichat, M. Sega, M. Vincenti, Environ. Sci. Technol. 29 (1995) 2226-2234.

[30] C. Minero, D. Vione, Appl. Catal. B-Environ. 67 (2006) 257-269.

[31] G. Camera-Roda, V. Augugliaro, A.G. Cardillo, V. Loddo, L. Palmisano, F. Parrino, F. Santarelli, Catal. Today 259 (2015) 87-96.

[32] C. Minero, V. Maurino, D. Vione “Photocatalytic mechanisms and reaction pathways drawn from kinetic and probe molecules”, in Photocatalysis and Water Purification: from Fundamentals to Recent Applications, 1th ed. – P. Pichat ed., 53-72, Wiley 2013.

[33] C. Minero, Catal. Today 54 (1999) 205-216.

[34] V. Maurino, A. Bedini, M. Minella, F. Rubertelli, E. Pelizzetti, C. Minero, J. Adv. Oxid. Technol. 11 (2008) 184-192.

[35] C. Minero, A. Bedini, V. Maurino, Appl. Catal. B-Environ. 128 (2012) 135-143.

[36] P. Wang, J. Wang, X. Wang, H. Yu, J. Yu, M. Lei, Y. Wang, Appl. Catal. B-Environ. 132-133 (2013) 452-459.

[37] W. Fan, Q. Lai, Q. Zhang, Y. Wang, J. Phys. Chem. C 115 (2011) 10694-10701.

[38] P. Calza, C. Hadjicostas, V.A. Sakkas, M. Sarro, C. Minero, C. Medana, T.A. Albanis, Appl. Catal. B-Environ. 183 (2016) 96-106.

[39] J. Ryu, W. Choi, Environ. Sci. Technol. 42 (2008) 294-300.

[40] R.J. Brandi, M.A. Citroni, M. Alfano, A.E. Cassano, Chem. Eng. Sci. 58 (2003) 979-985.

The complex interplay between adsorption and photoactivity in hybrids rGO/TiO_2

*M. Minella, F. Bertaina, C. Minero**

Department of Chemistry and NIS Center of Excellence, University of Torino, Via P. Giuria 5, Torino 10125, Italy http://www.environmentalchemistry.unito.it.

* Corresponding author. Tel. +39 0116708449, Fax +39-011-6705242; E-mail: claudio.minero@unito.it.

SUPPLEMENTARY MATERIAL

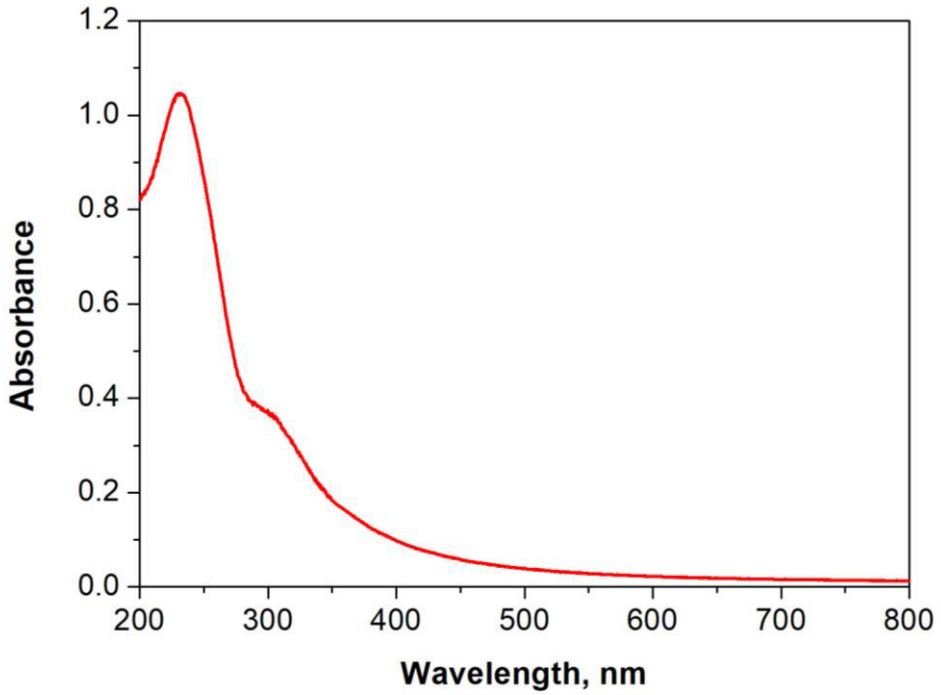

Fig. 1SM. Absorption spectrum of a GO suspension synthesized according to the method described in the main body of the text under paragraph 2.2.[1]

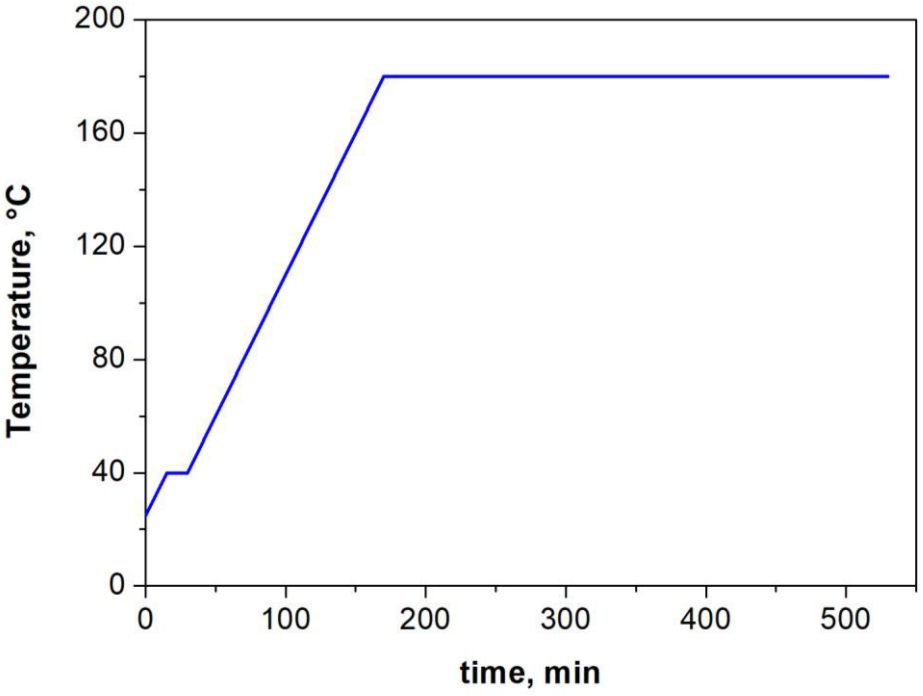

Fig. 2SM. Ramp profile adopted to carry out the hydrothermal reductive treatment in autoclave on suspension of TiO_2-GO at different loading. The hydrothermal condition allows the partial reduction of the GO oxidized moieties to give the desired TiO_2-rGO hybrids.

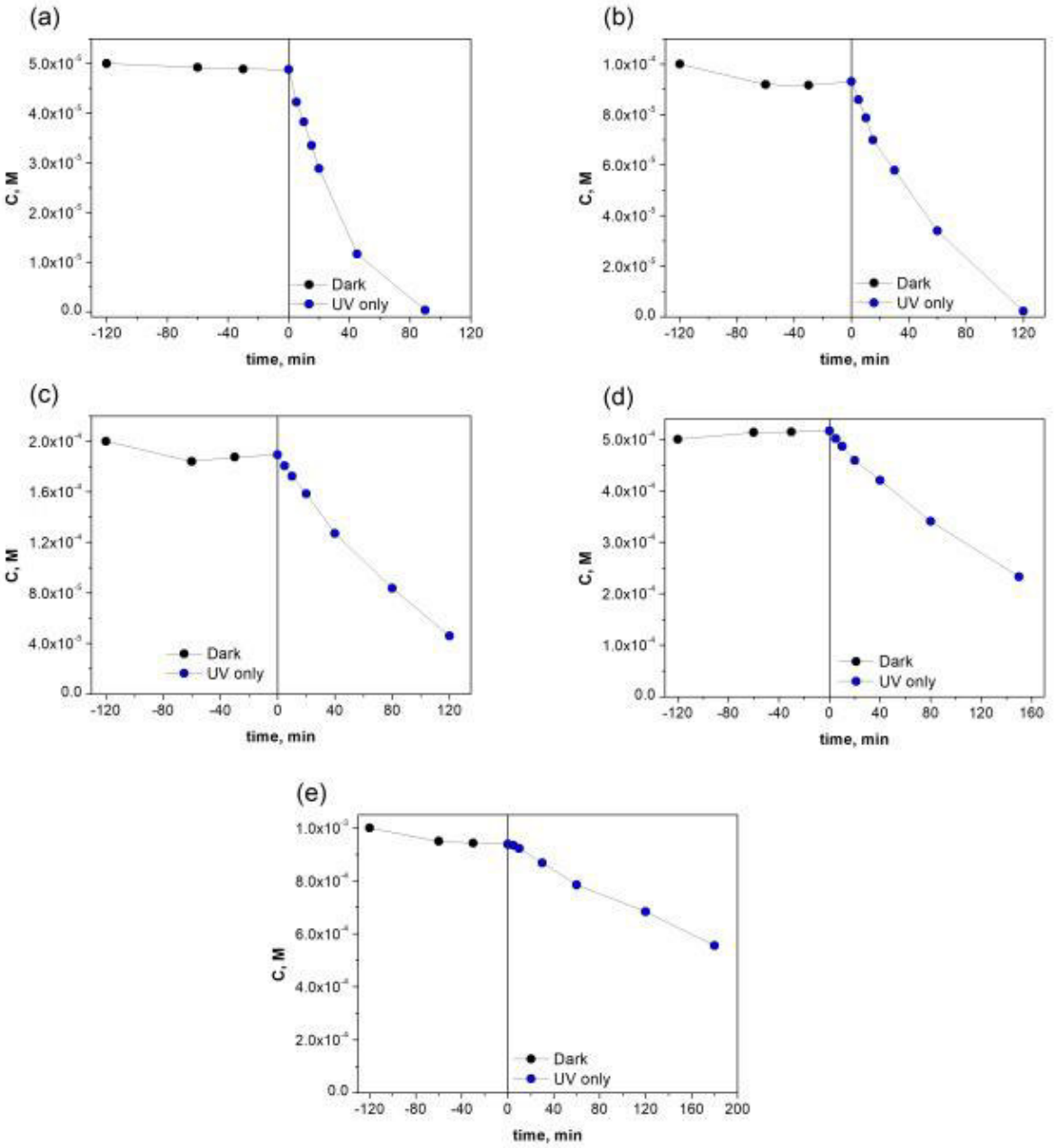

Fig. 3SM Adsorption (dark) and photocatalytic degradation (light) of 2,4-DCP on 0.5%rGO(HTR)-TiO_2 N100, at different initial concentration: (a) 5×10^{-5} M, (b) 1×10^{-4} M, (c) 2×10^{-4} M, (d) 5×10^{-4} M, (e) 1×10^{-3} M. Conditions: pH 3, [cat] = 500 mg/L, UV irradiation source (Philips 18W BLB lamp).

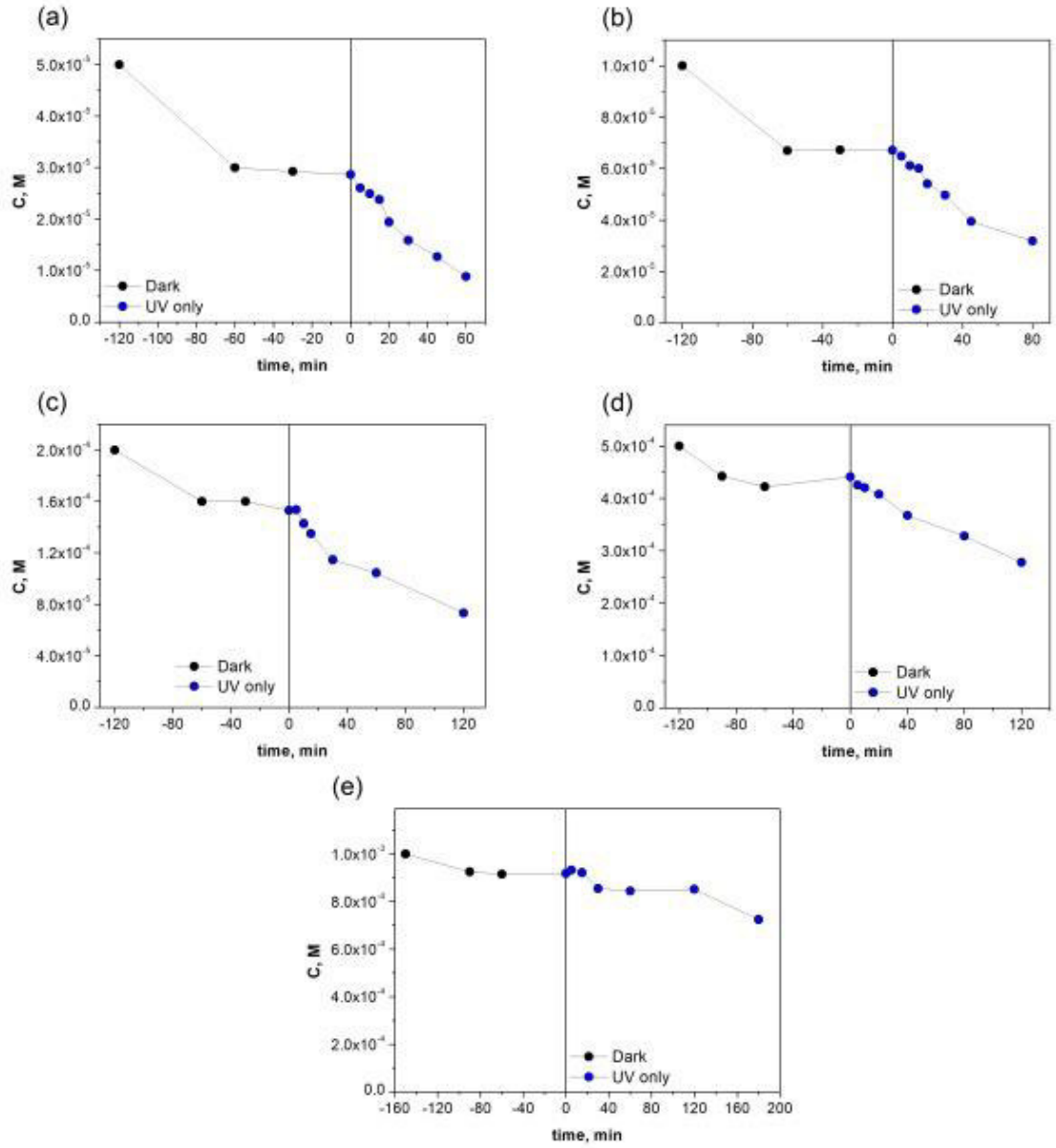

Fig. 4SM Adsorption (dark) and photocatalytic degradation (light) of 2,4-DCP on 10%rGO(HTR)-TiO_2 N100 at different initial concentration: (a) 5×10^{-5} M, (b) 1×10^{-4} M, (c) 2×10^{-4} M, (d) 5×10^{-4} M, (e) 1×10^{-3} M. Conditions: pH 3, [cat] = 500 mg/L, UV irradiation source (Philips 18W BLB lamp).

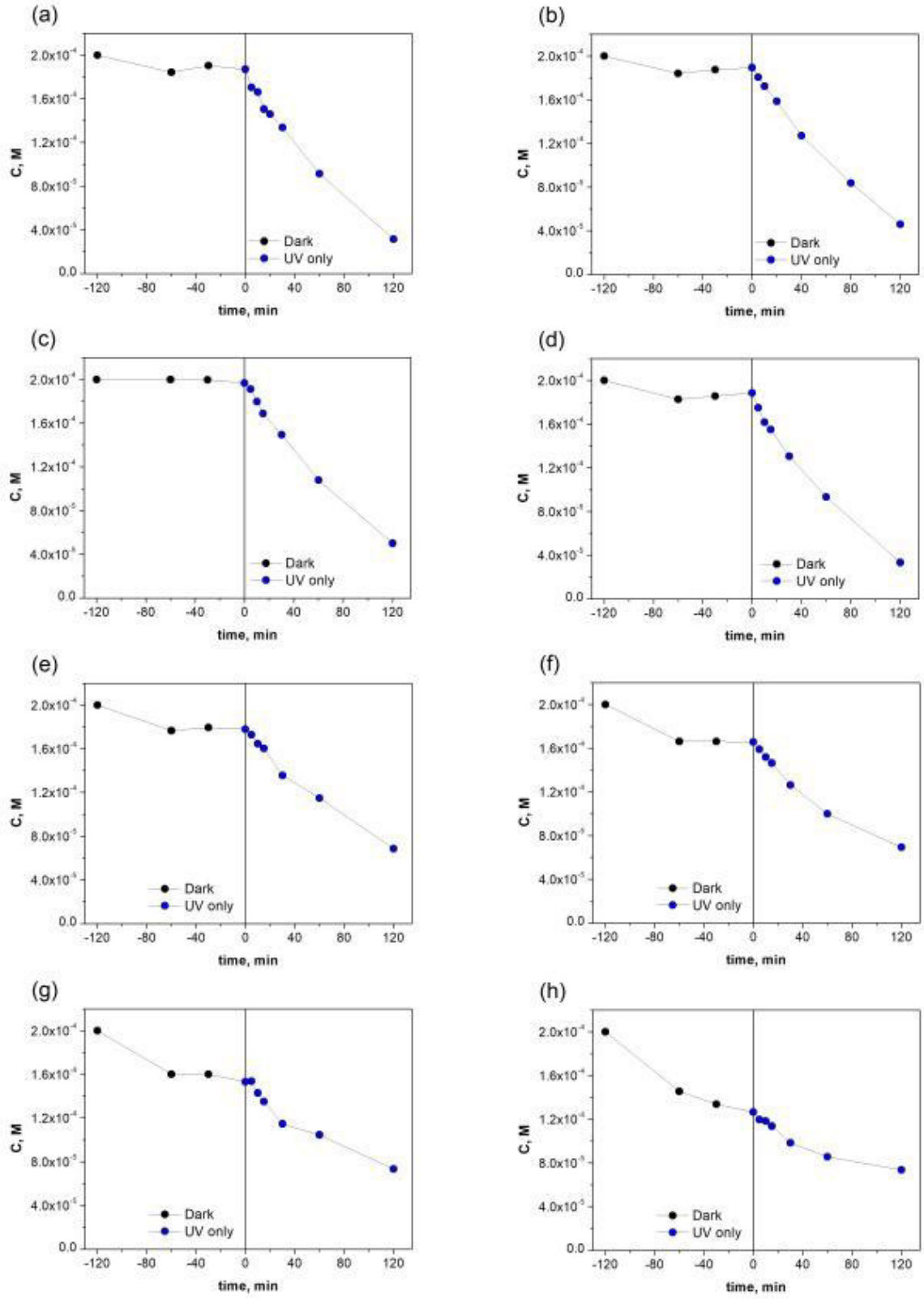

Fig. 5SM. Adsorption (dark) and photocatalytic degradation (light) of 2,4-DCP ($C_0 = 2\times10^{-4}$ M) in on (a) TiO_2 N100, (b) 0.5%rGO(HTR)–TiO_2 N100, (c) 1%rGO(HTR)–TiO_2 N100, (d) 2%rGO(HTR)–TiO_2 N100, (e) 4%rGO(HTR)–TiO_2 N100, (f) 6%rGO(HTR)–TiO_2 N100, (g) 10%rGO(HTR)–TiO_2 N100 and (h) 20%rGO(HTR)–TiO_2 N100. Conditions: pH 3, [cat] = 500 mg/L, UV only irradiation source (Philips 18W BLB lamp).

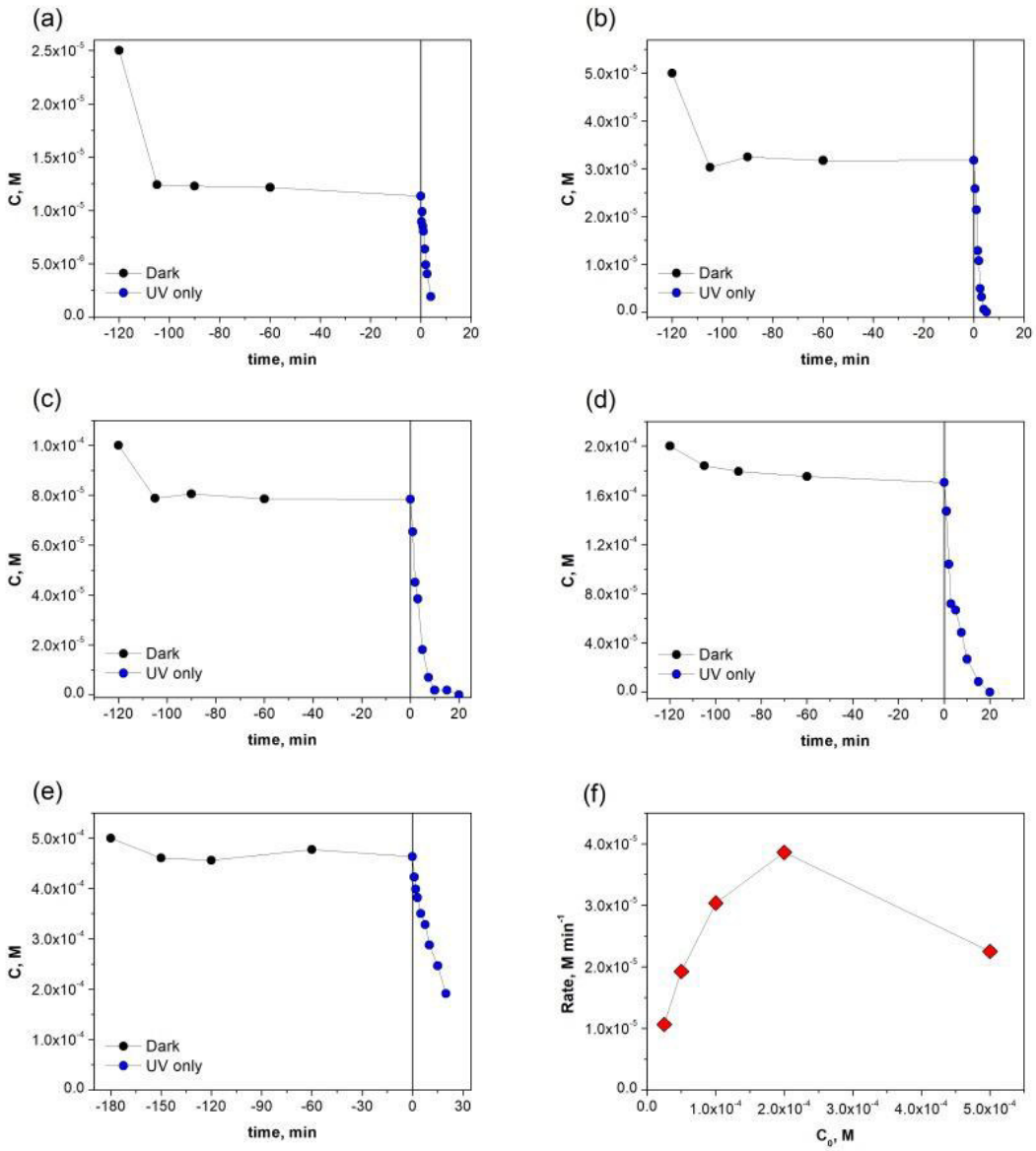

Fig. 6SM. Adsorption (dark) and photocatalytic degradation (light) of 1-naphthol at different initial concentration: (a) 2.5×10^{-5} M, (b) 5×10^{-5} M, (c) 1×10^{-4} M, (d) 2×10^{-4} M, (e) 5×10^{-4} M. Conditions: pH 3, [cat] = 500 mg/L, 2%rGO(CR)-TiO_2 N100, UV only irradiation source (Philips 18W BLB lamp).

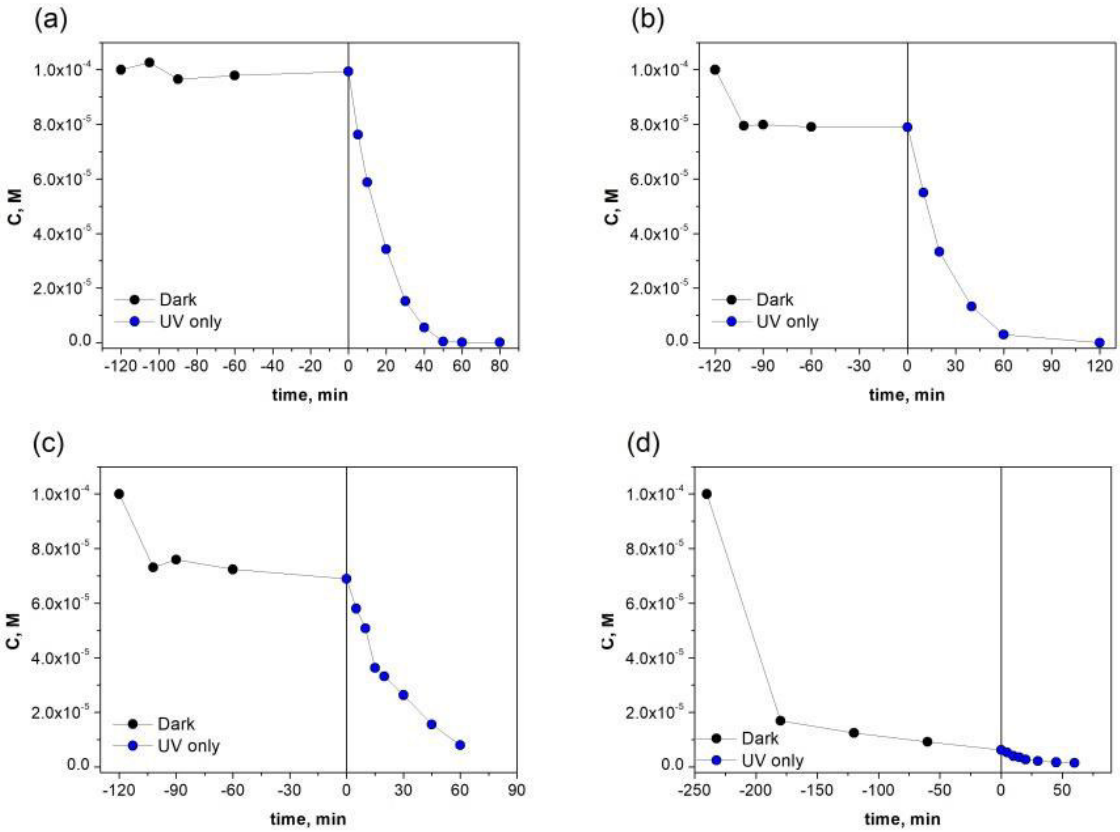

Fig. 7SM. Adsorption (dark) and photocatalytic degradation (light) of naphthol ($C_0 = 1\times10^{-4}$ M, pH 3, [cat] = 500 mg/L) on (A) TiO_2 N100, (B) 2%rGO(CR)-TiO_2 N100, (C) 6%rGO(CR)-TiO_2 N100 and (D) 10%rGO(CR)-TiO_2 N100. Irradiation source Philips TLK 03 (mainly visible, minor fraction UV).

1 References

[1] M. Minella, D. Versaci, S. Casino, F. Di Lupo, C. Minero, A. Battiato, N. Penazzi, S. Bodoardo, Electrochim. Acta 230 (2017) 132-140.